



**HAL**  
open science

# Importance of Vacancies and Doping in the Hole-Transporting Nickel Oxide Interface with Halide Perovskites

Boubacar Traoré, Laurent Pedesseau, Jean-Christophe Blancon, Sergei Tretiak, Aditya D Mohite, Jacky Even, Claudine Katan, Mikael Kepenekian

► **To cite this version:**

Boubacar Traoré, Laurent Pedesseau, Jean-Christophe Blancon, Sergei Tretiak, Aditya D Mohite, et al.. Importance of Vacancies and Doping in the Hole-Transporting Nickel Oxide Interface with Halide Perovskites. *ACS Applied Materials & Interfaces*, 2020, 12 (5), pp.6633-6640. 10.1021/ac-sami.9b19457 . hal-02472160

**HAL Id: hal-02472160**

**<https://univ-rennes.hal.science/hal-02472160v1>**

Submitted on 30 Mar 2020

**HAL** is a multi-disciplinary open access archive for the deposit and dissemination of scientific research documents, whether they are published or not. The documents may come from teaching and research institutions in France or abroad, or from public or private research centers.

L'archive ouverte pluridisciplinaire **HAL**, est destinée au dépôt et à la diffusion de documents scientifiques de niveau recherche, publiés ou non, émanant des établissements d'enseignement et de recherche français ou étrangers, des laboratoires publics ou privés.

1  
2  
3  
4  
5  
6  
7  
8  
9  
10  
11  
12  
13  
14  
15  
16  
17  
18  
19  
20  
21  
22  
23  
24  
25  
26  
27  
28  
29  
30  
31  
32  
33  
34  
35  
36  
37  
38  
39  
40  
41  
42  
43  
44  
45  
46  
47  
48  
49  
50  
51  
52  
53  
54  
55  
56  
57  
58  
59  
60

# Importance of vacancies and doping in hole transporting nickel oxide interface with halide perovskites

Boubacar Traore,<sup>\*,†</sup> Laurent Pedesseau,<sup>†</sup> Jean-Christophe Blancon,<sup>¶</sup> Sergei Tretiak,<sup>§</sup> Aditya D. Mohite,<sup>¶</sup> Jacky Even,<sup>†</sup> Claudine Katan,<sup>‡</sup> and Mikael Kepenekian<sup>\*,‡</sup>

<sup>†</sup>*Univ Rennes, INSA Rennes, CNRS, Institut FOTON - UMR 6082, F-35000 Rennes, France*

<sup>‡</sup>*Univ Rennes, ENSCR, CNRS, ISCR – UMR 6226, F-35000 Rennes, France*

<sup>¶</sup>*Department of Chemical and Biomolecular Engineering, Rice University, Houston, TX 77005.*

<sup>§</sup>*Los Alamos National Laboratory, Los Alamos, NM 87545, U.S.A.*

E-mail: boubacar.traore@insa-rennes.fr; mikael.kepenekian@univ-rennes1.fr

## Abstract

Nickel oxide (NiO) is a commonly used contact material for a variety of thin-film optoelectronic technologies based on organic or hybrid materials. In such setups, interfaces play a crucial role as they can reduce, if not kill, the device performances by bringing additional traps or energy barriers hindering charge carriers extraction from the active layer. Here, we computationally examine a prototype halide perovskite architecture, NiO/MAPbI<sub>3</sub> (MA = CH<sub>3</sub>NH<sub>3</sub><sup>+</sup>), which has shown excellent photovoltaic performance and in particular a large open-circuit voltage. We show that efficient hole collection is only achieved when considering the role of vacancies induced by standard material deposition techniques. Specifically, Ni vacancies lead to nearly perfect valence band energy level alignment between the active layer and the contact material. Finally, we show how Li doping greatly improves the performances of the device and further propose alternative dopants. Our results suggest the high tunability of NiO interfaces for the design of optimized optoelectronic devices far beyond halide perovskites.

## Introduction

Tuning interface energetics in thin film optoelectronic devices is of paramount importance. In such devices, the photo-active material is typically sandwiched between charge collection layers, which are referred to as electron transport layer (ETL) and hole transport layer (HTL). Poorly matched and designed interfaces can lead to energy level and dielectric mismatches along with traps causing undesired charge carriers recombination that may overall reduce the performances of the photo-active layer.<sup>1,2</sup> Hence, their selection and optimization play an essential role in the performance of optoelectronic devices.<sup>2-4</sup> Among HTL materials, the inorganic transition metal-oxide nickel oxide (NiO), is an attractive technological and relatively inexpensive solution including low-cost solution process deposition techniques.<sup>5</sup> Its adoption in photovoltaics was triggered by the pioneering works of He *et al.*<sup>6</sup> and Irwin *et al.*<sup>7</sup> in dye-sensitized solar cells (DSSC) and organic photovoltaic (OPV) devices, respectively. Moreover, NiO finds extensive applications as a transparent conductive oxide,<sup>8</sup> in water splitting<sup>9</sup> and batteries.<sup>10</sup> The interest for NiO in these diversified fields takes root from its wide band gap ( $> 3.6$  eV), *p*-type conduction and magnetic and optical refraction properties.

Recently, some of those features were exploited in the context of hybrid organic-inorganic perovskites (HOP) based optoelectronic devices. These studies have been motivated by the power conversion efficiency of HOP-based photovoltaics, which nowadays competes with that of silicon solar cells.<sup>11</sup> In particular, HOP solar cells exhibit attractive photovoltaic performances when NiO is used as a HTL in stable large-area architectures or monolithic HOP/silicon tandem devices.<sup>12-16</sup> The improved performance was attributed to the near ideal valence band energy alignment between NiO and, for instance, methylammonium (MA =  $\text{CH}_3\text{NH}_3^+$ ) lead iodide  $\text{MAPbI}_3$ .<sup>17,18</sup> Besides, the experimental measurements point to an increased photovoltaic power conversion efficiency when NiO is doped with Li.<sup>18</sup> Few theoretical works describe the interface of halide perovskites with  $\text{TiO}_2$ ,<sup>19</sup> even fewer deal with other HTL.<sup>20</sup> As a consequence, the fundamental understanding of the origin of such a

1  
2  
3 near ideal alignment between NiO and MAPbI<sub>3</sub> with and without Li doping is lacking.  
4

5 Here, we study an archetypal interface through first-principle calculations based on den-  
6 sity functional theory (DFT) by examining in detail NiO junctions with the prototypical HOP  
7 material, MAPbI<sub>3</sub>. Considering the defect-free interface, we find that the high-frequency di-  
8 electric constant profile across the interface presents a low dielectric contrast between the  
9 two materials, which benefits hole extraction. However, our results show that the valence  
10 band energy level alignment between pristine NiO and MAPbI<sub>3</sub> materials is not favourable  
11 for hole extraction. In contrast, we show a significant change in the valence band energetics  
12 of NiO due to native Ni vacancies appearing in the material deposition. This is consistent  
13 with ultraviolet photoelectron spectroscopy (UPS) experiments. Therefore, we demonstrate  
14 that the widely accepted view of near ideal experimental valence band energy level alignment  
15 between NiO and MAPbI<sub>3</sub> is related to these Ni vacancies. Finally, we show that Li doping  
16 improves the level alignment and propose Cs and Rb as alternative dopants of NiO to fur-  
17 ther tune its interfacial energetics. The methodology developed in this report will be directly  
18 transferable to the understanding of other types of interfaces including various perovskites,  
19 conventional semiconductors, and alternative carrier transport layer materials.  
20  
21  
22  
23  
24  
25  
26  
27  
28  
29  
30  
31  
32  
33  
34  
35  
36

## 37 Results and discussion

38  
39  
40 **NiO and MAPbI<sub>3</sub> bulk materials** NiO is a prototype transition metal oxide that has  
41 been extensively scrutinized over the years.<sup>21–24</sup> The localized Ni 3d electrons make it a highly  
42 correlated system, whose theoretical description fails in the local density approximation  
43 (LDA) or the generalized gradient approximation (GGA) of DFT.<sup>25</sup> Hence, we adopted the  
44 so-called LDA+U (or GGA+U) method<sup>26,27</sup> by applying a Hubbard-like correction term U  
45 to Ni 3d orbitals within the SIESTA code (see Supporting Information, SI).<sup>28,29</sup> In previous  
46 works, the method has been successful in describing the magnetic properties of NiO and  
47 results in a band gap that is in a fair agreement with experiment.<sup>26,27</sup> In our case, we found  
48  
49  
50  
51  
52  
53  
54  
55  
56  
57  
58  
59  
60

1  
2  
3 that an effective  $U$  value ( $U_{\text{eff}}$ ) of 6.0 eV was well suited to capture the main features of  
4 the electronic structure of NiO and is consistently used across the different calculations for  
5 comparison. We note that this value falls within the accepted range of appropriate  $U$  values  
6 reported for NiO in the literature.<sup>27,30</sup> The detailed description of the electronic structure  
7 of NiO and the selection of  $U_{\text{eff}}$  can be found in the SI (Text S1). Briefly, the electronic  
8 band gap of NiO corresponds to a charge transfer type excitation (Text S2, SI) and the  
9 calculated magnetic moment of Ni ( $1.77 \mu_B$ ) is in excellent agreement with the experimental  
10 value ( $\sim 1.7 \mu_B$ ).<sup>31</sup> Moreover, the computed relaxed lattice constant ( $a = 4.25 \text{ \AA}$ ) presents  
11 less than 2% error as compared to the experimental structure ( $a = 4.167 \text{ \AA}$ ).<sup>32</sup>

21 The MAPbI<sub>3</sub> perovskite and its alloys, involving formamidinium cations and mixed  
22 cations/halides, have so far produced the most efficient solar cells.<sup>33,34</sup> Structurally, MAPbI<sub>3</sub>  
23 forms a 3-dimensional lattice where corner-shared PbI<sub>6</sub><sup>2-</sup> octahedra extend in all directions  
24 with MA cation tumbling around the center of the cubo-octahedra. Over the past years,  
25 impressive chemical and materials engineering of HOP have been carried out not only to in-  
26 crease their efficiencies but also to improve their stabilities and photophysical properties.<sup>2,16</sup>  
27 Here, we use its orthorhombic phase with well-defined positions of MA in order to avoid the  
28 issue of the dynamical disorder of the latter in the tetragonal and cubic structures.<sup>35</sup> This  
29 low-temperature phase has been extensively studied and DFT-based calculations provide a  
30 correct description of the main electronic features, in particular, the direct bandgap at  $\Gamma$   
31 point (Figure S2, SI). Let us note that, because of the presence of the heavy atom Pb, the  
32 correct treatment of MAPbI<sub>3</sub> should include spin-orbit coupling (SOC). However, the impact  
33 of SOC on valence band states is negligible (Figure S2, SI), thus it is reasonable to neglect  
34 SOC in our DFT calculations focusing on the NiO/MAPbI<sub>3</sub> interface for hole extraction only  
35 (spin polarization, however, is included).

52 **NiO/MAPbI<sub>3</sub> pristine interface** Considering the experimentally observed (100) surface  
53 of NiO and corresponding lattice parameters,<sup>31,32</sup> the MAPbI<sub>3</sub> (010) surface affords appro-

1  
2  
3 appropriate lattice matching for a NiO/MAPbI<sub>3</sub> interface (Table S3, SI). The resulting lateral  
4 lattice mismatch between MAPbI<sub>3</sub> and NiO is less than 3%. Details related to the interface  
5 construction can be found in Text S3 (SI).  
6  
7

8  
9 To combine NiO and MAPbI<sub>3</sub> at the interface, we terminated MAPbI<sub>3</sub> by MAI (Figure 1a)  
10 as suggested by STM measurements<sup>36</sup> and reported to be the favourable termination using  
11 DFT.<sup>37</sup> The interface relaxes such that iodine atoms point towards nickel atoms (Figure 1b)  
12 with a Ni-I bond length of about 2.87 Å, in good agreement with bulk Ni-I bond distance of  
13 2.78 Å in hexagonal R-3m NiI<sub>2</sub>.<sup>38</sup> The resulting band structure (Figure 1c) shows a direct  
14 band gap at  $\Gamma$  point. The wavefunction plot of the valence band maximum (VBM) at  $\Gamma$   
15 point reveals an anti-bonding hybridization between Pb(6s)-I(5p) states only (Figure 1d),  
16 whereas the same band shows NiO states at the in-plane M<sub>xy</sub> point. Stated differently,  
17 hole wavefunctions are localized inside the perovskite at  $\Gamma$  point while they are delocalized  
18 between both the perovskite and NiO at M<sub>xy</sub> point. The presence of I states at M<sub>xy</sub> point is  
19 consistent with Ni-I bond formation and shows an efficient coupling between MAPbI<sub>3</sub> and  
20 NiO.  
21  
22  
23  
24  
25  
26  
27  
28  
29  
30  
31  
32

33 Efficient charge separation in solar cell devices, and more generally semiconductor het-  
34 erostructures, depends on the dielectric properties of the respective materials. If the paired  
35 media have different dielectric constants, charge separation through the interface and the  
36 subsequent carrier transport may be improved or frustrated depending on the extent of the  
37 dielectric mismatch.<sup>1</sup> In our NiO/MAPbI<sub>3</sub> interface, we evaluated the dielectric constants  
38 by considering the high-frequency component ( $\epsilon_{\infty}$ ) along the interface direction using a first-  
39 principle based approach described elsewhere.<sup>39,40</sup> Figure 2 shows the profile of  $\epsilon_{\infty}$  along  
40 the interface through NiO and MAPbI<sub>3</sub> layers. In their central bulk-like regions, both NiO  
41 ( $\epsilon_{\infty} = 5.1$ ) and MAPbI<sub>3</sub> ( $\epsilon_{\infty} = 5.4$ ) have values that are comparable to those calculated  
42 for their bulk experimental structures (Figure S4, SI). The calculated values for NiO and  
43 MAPbI<sub>3</sub> are also in a good agreement with the experimentally measured values amount-  
44 ing to 5.7 and 6.5, respectively.<sup>41,42</sup> At the interface region, the dielectric constant shows  
45  
46  
47  
48  
49  
50  
51  
52  
53  
54  
55  
56  
57  
58  
59  
60

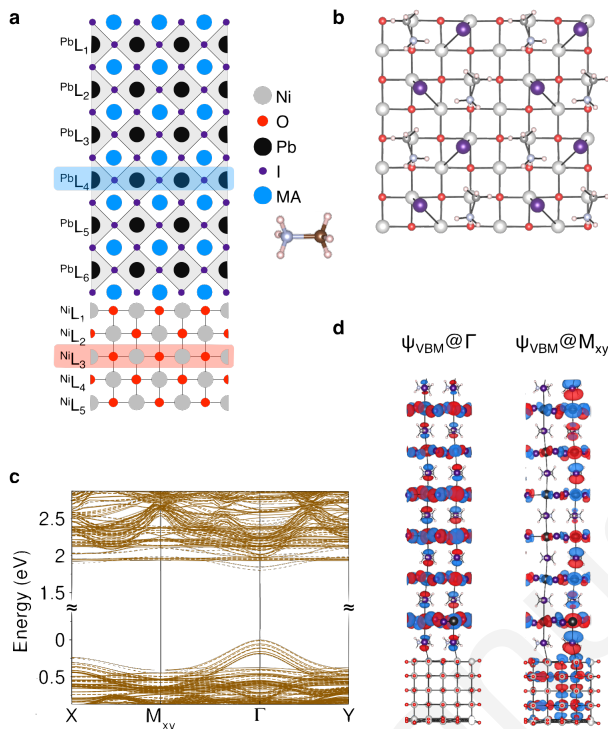


Figure 1: Lattice structure and electronic properties of the NiO/MAPbI<sub>3</sub> interface. **a** Model used in our calculations and layer labels. **b** Favorable iodine positions at the interface with I atoms pointing towards Ni in a bridge-like configuration. Here I, Ni, O, N, C and H atoms are depicted in purple, light gray, red, blue, dark gray and pale pink colors, respectively. **c** Band structure of the relaxed interface model with a direct bandgap at  $\Gamma$  point. The valence band maximum (VBM) at  $\Gamma$  point is taken as the energy reference. Plain and dashed lines correspond to majority and minority spins, respectively. **d** VBM Wavefunction at  $\Gamma$  and  $M_{xy}$  points. Hybridized MAPbI<sub>3</sub> and NiO states appear at  $M_{xy}$  point while MAPbI<sub>3</sub> dominate at  $\Gamma$  point.

a local peak, which is, to some extent, related to the NiO interface states that hybridize with those of MAPbI<sub>3</sub>, resulting in an interface dipole that we estimated to be about 2.0 Debye. Interestingly, the two dielectric constants ( $\epsilon_{\infty}$ ) are comparable indicative of a low dielectric contrast/mismatch between MAPbI<sub>3</sub> and NiO. This may hint to an efficient charge separation across the interface due to possible reduced binding energy of holes as a result of low dielectric mismatch.<sup>1</sup> Noteworthy, in the actual room temperature solar cell operation, low-frequency static dielectric constant ( $\epsilon_s$ ) also plays an important role and may represent a dominant contribution in the response of charge carriers to the electric field.<sup>43</sup> Effective  $\epsilon_s$  values ranging from 11–20 can be expected in MAPbI<sub>3</sub> due to optical phonons and rotational tumbling of organic cations,<sup>43,44</sup> whereas this value amounts to 11.90 for NiO.<sup>41</sup>



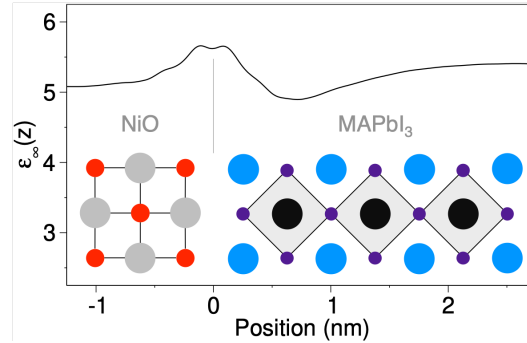


Figure 2: High-frequency dielectric constant profile of the NiO/MAPbI<sub>3</sub> interface. The dielectric mismatch is low, which points to efficient charge extraction at the interface. The inset shows the corresponding position of the NiO/MAPbI<sub>3</sub> slab.

For an efficient hole transmission from the perovskite layer to the hole transport material, the VBM of the latter should be above that of the former. A parameter that quantifies the shift between the VBM of the heterostructure materials is referred to as the valence band offset (VBO). Here, it is defined as the difference between  $\text{VBM}_{\text{NiO}}$  and  $\text{VBM}_{\text{MAPbI}_3}$  from their bulk-like layers.<sup>45</sup> Therefore, positive values for VBO indicate that NiO states stand higher in energy than the respective MAPbI<sub>3</sub> states, an ideal situation for hole extraction. In contrast, negative values lead to an unfavourable interface for solar cell applications. Our calculations imply the presence of MAPbI<sub>3</sub> states above those of NiO (Figure 1c) pointing to a valence band energy level alignment that is detrimental for hole collection. This is confirmed by a layer resolved projected density of states (PDOS, Figure 3a). Indeed, from the PDOS, one can extract the position of the VBM of the layers emulating the bulk of both materials ( $^{\text{Ni}}\text{L}_3$  for NiO and  $^{\text{Pb}}\text{L}_4$  for MAPbI<sub>3</sub>, Figure 1a). In the case of the MAPbI<sub>3</sub>/NiO interface, from the PDOS we obtain a VBO of about  $-0.41$  eV between MAPbI<sub>3</sub> and NiO (Figure 3). We obtain a similar VBO ( $-0.36$  eV) using the Hartree potential alignment<sup>46</sup> (Text S4 and Figure S5, SI) showing that both the PDOS and the Hartree potential alignment methods can be used to compute band offsets.<sup>45,47</sup> Surprisingly, the sign of our calculated VBO value seemingly contradicts the experimental findings, which point to an almost ideal VBO (ranging from  $+0.0$  to  $+0.4$  eV) between MAPbI<sub>3</sub> and NiO making the latter a suitable material for hole extraction and transport.<sup>14,18,48,49</sup>

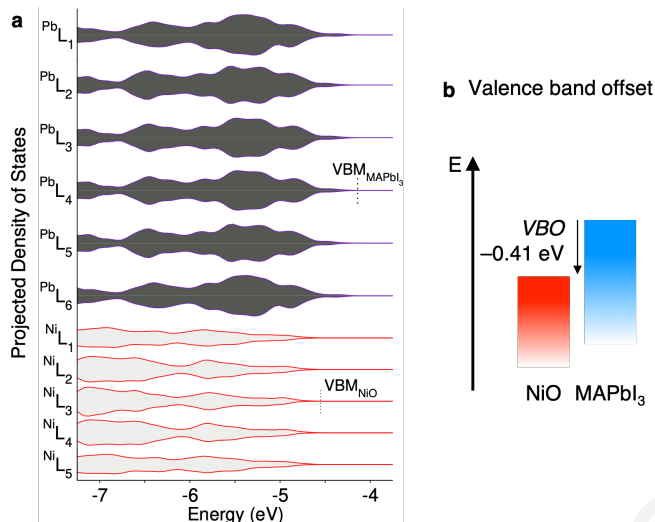


Figure 3: Valence band alignment in the NiO/MAPbI<sub>3</sub> pristine interface. **a** Layer-by-layer projected density of states (PDOS) of the relaxed interface model affording valence band alignment from the bulk-like parts of MAPbI<sub>3</sub> and NiO. **b** The valence band offset (VBO) determined from the PDOS. The computed VBO is not favourable for hole extraction.

Since this finding contrasts to experimental results, we checked that it was neither an artifact of the choice of the starting orthorhombic structure nor the considered number of layers in MAPbI<sub>3</sub> or our computational approach. Firstly, we obtained similar results with tetragonal MAPbI<sub>3</sub> as the starting structure of the interface (Text S5 and Figure S6, SI) and by increasing the number of layers in both MAPbI<sub>3</sub> and NiO (Text S6 and Figure S7, SI). Then, we recalculated the electronic structure using the GGA+U formalism in plane-wave basis sets instead of localized basis sets (Text S7, SI). These new simulations lead to a negative VBO of  $-0.53$  eV, confirming the counterintuitive result. Hybrid functional calculations (HSE03<sup>50</sup> and HSE06<sup>51</sup>) also confirm the trend (VBO  $\approx -0.70$  eV). Thus, the sign of VBO is not an artifact of the Hubbard correction approach (Text S8, SI).

While the DFT approach is not responsible for the sign of the VBO, it might be influenced by the structural choices made in the construction of NiO/MAPbI<sub>3</sub> interface. Indeed, despite that STM experiments point to a MAI-termination in MAPbI<sub>3</sub>,<sup>36</sup> PbI termination may not be completely excluded as it is reported to be slightly more stable by other first-principles simulations.<sup>52,53</sup> To assess the possible effect of this termination on the electronic structure of

1  
2  
3 the NiO/MAPbI<sub>3</sub> interface model, we considered the same interface but with PbI termination  
4 (Text S9 and Figure S11, SI). We find that the most stable configuration presents a VBO  
5 shift of  $-0.15$  eV with MAPbI<sub>3</sub> states above those of NiO indicative of an unfavorable  
6 alignment for hole collection. We note that in real thin films, several interface configurations  
7 may co-exist depending on the deposition technique and conditions. This could eventually  
8 lead to the formation of some metastable domains in the device, thus affecting the interfacial  
9 energetics (Figure S12, SI). However, we hypothesize that the thermodynamics of the system  
10 should make the favorable energy configurations to dominate.

11  
12  
13  
14  
15  
16  
17  
18  
19 Finally, considering the effect of substituting the cation in the perovskite layer, we also  
20 inspected the energy level alignment of FAPbI<sub>3</sub>/NiO interface (Text S10, SI) with FA refer-  
21 ring to Formamidinium (FA = CH(NH<sub>2</sub>)<sub>2</sub>). Here, we used the (001) surface of cubic FAPbI<sub>3</sub>  
22 with FAI termination and lattice-matched it to NiO, the latter being the substrate. We  
23 calculated a VBO of  $-0.15$  eV with FAPbI<sub>3</sub> states above those of NiO (Figure S13, SI).  
24 As in MAPbI<sub>3</sub>, this VBO is not optimal for hole collection from FAPbI<sub>3</sub> to NiO. However,  
25 the absolute value of this shift is lower as compared to  $-0.41$  eV obtained with MAPbI<sub>3</sub>.  
26 Detailed information on this interface, the related discussion on the lower VBO with FAPbI<sub>3</sub>  
27 and possible effects of mixed cation HOP on the properties of this interface can be found in  
28 Text S10 (SI). In the end, all these results confirm a valence band energy level alignment that  
29 is not in favour of efficient hole collection when considering defect-free interfaces of pristine  
30 materials.

31  
32  
33  
34  
35  
36  
37  
38  
39 Hence, a legitimate question about the possible origin of this apparent contradiction  
40 arises. Could it be related to the assumption of the defect-free NiO and MAPbI<sub>3</sub> lattices in  
41 our model? What is the role of doping in the experimentally reported VBO? In the following,  
42 we aim to address these questions.

43  
44  
45  
46  
47  
48  
49  
50  
51  
52 **Role of vacancies** Despite hybrid perovskites being referred to as "defect-tolerant",<sup>54-56</sup>  
53 various defects are abundant in these materials and their role on the interfacial properties of  
54  
55  
56  
57  
58  
59  
60

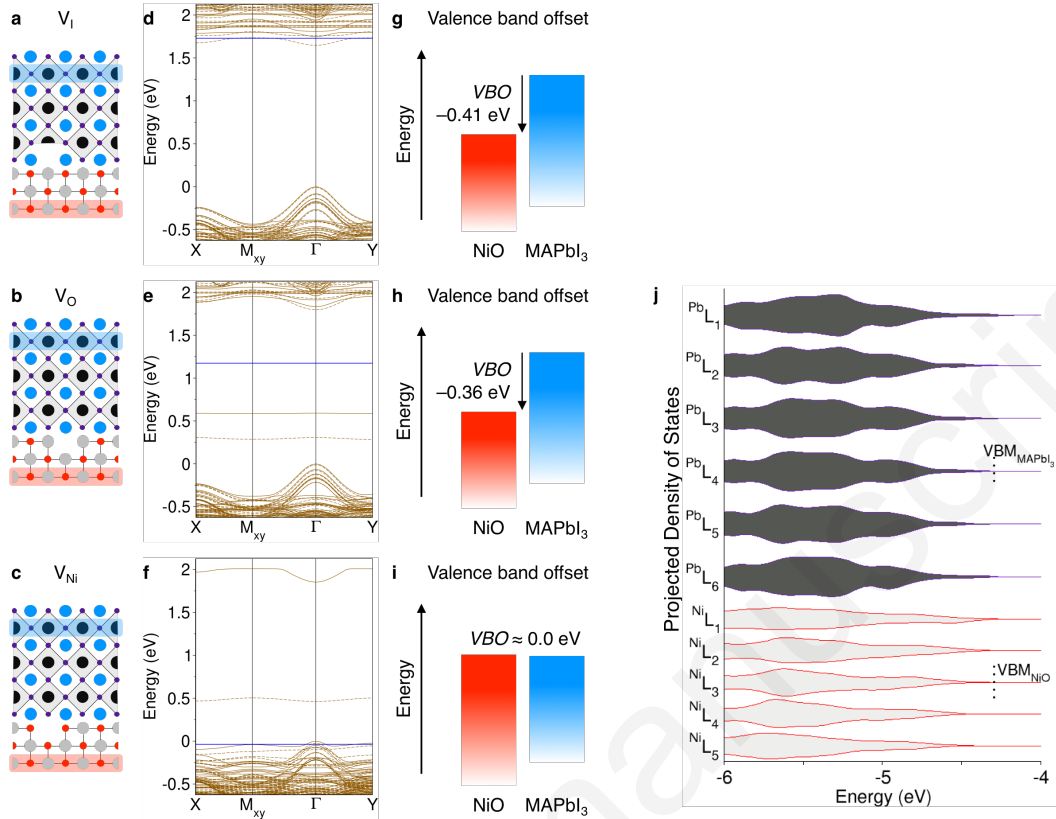


Figure 4: Role of vacancies in the NiO/MAPbI<sub>3</sub> interface. **a**, **b**, **c** Iodine ( $V_I$ ), oxygen ( $V_O$ ) and nickel ( $V_{Ni}$ ) vacancy models, respectively. **d**, **e**, **f** Corresponding calculated band structures. The valence band maximum at  $\Gamma$  point is taken as the energy reference, a blue line marks the Fermi level. Plain and dashed lines correspond to majority and minority spins, respectively. **g**, **h**, **i** Corresponding computed valence band offsets. **j** Layer by layer projected density of states (PDOS) of the interface model with  $V_{Ni}$  resulting in the VBO shown in **i**. Nickel vacancies produce a valence band alignment favourable to hole extraction.

MAPbI<sub>3</sub> remains elusive. While it is of great fundamental and technological interest, there is no theoretical study of their effects on the electronic structure of NiO/MAPbI<sub>3</sub> interface, which we address in this section. To introduce defects and later dopants into the interface model, we enlarge the defect-free cell in order to reduce the effects of spurious interactions, originating from the periodic boundary conditions, on the computed properties (see Text S11, SI). We consider the impact of different defects that could potentially influence the valence band alignment: iodine vacancies ( $V_I$ , Figure 4a), oxygen vacancies ( $V_O$ , Figure 4b) and nickel vacancies ( $V_{Ni}$ , Figure 4c). Furthermore, MA vacancies ( $V_{MA}$ ), Pb vacancies ( $V_{Pb}$ ) and Schottky-type defect MAI vacancies ( $V_{MAI}$ ) are presented in the SI (Text S11, SI).

1  
2  
3 The band structure of  $V_I$  (Figure 4d) shows a shallow defect level at the conduction band,  
4 in agreement with previous results,<sup>57</sup> while having negligible effect on the valence band. In  
5 the case of  $V_O$ , localized mid-gap trap states are formed. The analysis of the wavefunctions  
6 shows that these states arise from Ni atoms in direct contact with the vacant oxygen site.  
7 Such mid-gap states are a source of non-radiative recombinations detrimental to photovoltaic  
8 performances. However, similar to  $V_I$ , the presence of  $V_O$  brings no change to the shape  
9 of the valence bands. Both  $V_I$  and  $V_O$  barely affect the VBO of the interface model as  
10 compared to the defect-free cell and we obtain a negative value of *ca.*  $-0.40$  eV for the two  
11 systems (Figure 4g,h).  
12  
13  
14  
15  
16  
17  
18  
19  
20

21 Similarly, we calculate a VBO of *ca.*  $-0.31$  eV for  $V_{MAI}$  with the valence band barely  
22 affected (Figure S15, SI).  $V_{MA}$  and  $V_{Pb}$  at the interface region ( $^{Pb}L_6$ ) present a VBO of  
23  $-0.05$  eV and  $-0.10$  eV, respectively and the Fermi level is shifted to the valence bands  
24 forming shallow acceptor states in agreement with previous reports (Figures S16-S19, SI).<sup>58,59</sup>  
25 In the bulk-like region of  $MAPbI_3$  ( $^{Pb}L_4$ ), VBO of  $V_{MA}$  and  $V_{Pb}$  become *ca.*  $-0.46$  eV and  
26 *ca.*  $-0.41$  eV, respectively (Figures S17 and S19, SI). Hence with  $MAPbI_3$  related defects  
27 along with  $V_O$ , VBO remain essentially unfavorable for hole collection across  $NiO/MAPbI_3$   
28 interface.  
29  
30  
31  
32  
33  
34  
35  
36

37 On the other hand, the presence of a  $V_{Ni}$  site at both the interface and bulk-like layers  
38 ( $^{Ni}L_1$  and  $^{Ni}L_3$ ), is accompanied by the emergence of less dispersive bands (Figure 4f and  
39 Figure S20, SI) that are localized on O atoms (2p states) around  $V_{Ni}$  and the next neighbor Ni  
40 atoms (3d states). Noteworthy, it results in a large positive energy shift of the valence bands  
41 related to NiO, which becomes almost equals to the VBM of the  $MAPbI_3$  (Figure 4f and  
42 Figures S20-S22, SI). As a consequence, the VBO becomes almost vanishing (Figure 4i,j)  
43 and the material system becomes *p*-type (Fermi energy crosses the valence states). The  
44 latter result is in agreement with the valence band alignments given in the literature between  
45  $MAPbI_3$  and NiO.<sup>14,49</sup> It is known that  $V_{Ni}$  makes NiO become a *p*-type semi-conductor,<sup>60,61</sup>  
46 but its effect on the interfacial properties of  $MAPbI_3$  has not been assessed previously. This  
47  
48  
49  
50  
51  
52  
53  
54  
55  
56  
57  
58  
59  
60

1  
2  
3 is an important point: It indicates that the presence of  $V_{\text{Ni}}$  in NiO with MAPbI<sub>3</sub> is probably  
4 at the origin of the measured near-ideal energy alignment between the two materials. This  
5 is plausible considering the standard fabrication processes (sputtering, spin-coating etc.) of  
6 NiO as this oxide is experimentally known to be generally Ni deficient.<sup>62</sup>  
7  
8  
9

10  
11  
12 **Experimental confirmation** The reported experimental energy level alignments between  
13 NiO and MAPbI<sub>3</sub> generally, if not all, rely on the difference between the work functions ( $W_F$ )  
14 of NiO and the absolute valence band energy (AVBE) of MAPbI<sub>3</sub>. While the AVBE of *ca.*  
15  $-5.4$  eV for MAPbI<sub>3</sub> seems more consensual in the realm of reported data,<sup>63</sup> the measured  
16  $W_F$  for NiO largely depends on the processing conditions and NiO surface exposure.<sup>64</sup> Re-  
17 ported  $W_F$  values fall between  $-5.0$  eV to  $-5.6$  eV,<sup>5,7,64-66</sup> reaching as high as  $-6.2$  eV to  
18  $-6.7$  eV in pure NiO film deposited in-situ.<sup>64</sup> For a purely processed NiO film, its  $W_F$  can be  
19 assumed to be close in value to its AVBE as its purity makes it stoichiometric with no defect.  
20 Indeed, the measured UPS absolute valence band energy of  $-6.5$  eV<sup>67,68</sup> for NiO agrees well  
21 with the  $W_F$  of purely deposited NiO. Hence, using an AVBE of  $-6.2$  eV to  $-6.5$  eV for NiO  
22 to align it with MAPbI<sub>3</sub>, the resulting VBO gives  $-0.8$  eV to  $-1.1$  eV, which is in a good  
23 agreement with our prediction for the defect-free NiO/MAPbI<sub>3</sub> interface model (Figure 3b).  
24 Moreover, considering  $W_F$  of NiO in air-exposed conditions (*ca.*  $-5.4$  eV), with potential  
25 defects like Ni vacancies,<sup>62</sup> we recover the literature reported near-ideal valence band align-  
26 ment between NiO and MAPbI<sub>3</sub>. This is in a good agreement with our predictions on the  
27 role of Ni vacancies in turning NiO into a *p*-type material in the interface model. Therefore,  
28 we believe that the experimentally reported deposited NiO films via sputtering/spin-coating  
29 during HOP fabrication present dominant Ni vacancies,<sup>62</sup> which appear to help the perfor-  
30 mances of nickel-based perovskite solar cells. However, the appearance of the less-dispersive  
31 mid-gap defect-like states due to the presence of  $V_{\text{Ni}}$  at the interface can alleviate the ef-  
32 ficiency of hole carrier collection at the NiO/MAPbI<sub>3</sub> interface. Since all the investigated  
33 defects, except  $V_{\text{Ni}}$ , lead to a negative VBO, we postulate that increasing their concentration  
34  
35  
36  
37  
38  
39  
40  
41  
42  
43  
44  
45  
46  
47  
48  
49  
50  
51  
52  
53  
54  
55  
56  
57  
58  
59  
60

would only worsen the properties of this interface. Therefore, it is desirable to limit and/or reduce their concentration inside the film while, at the same time, preserving an ideal energy alignment. A practical strategy to achieve that goal is by doping, which is discussed in the next section.

**Role of doping** Similar to other semiconductors, doping strategies have been used to fine-tune the properties of NiO, notably using Li for improved  $p$ -conductivity<sup>69,70</sup> and solar efficiencies in perovskites.<sup>18,71</sup> To bring more fundamental understanding to this improvement, we study the effect of Li doping of NiO by considering the substitution in our simulation cell of 2 Ni atoms, chosen as far from each other as possible, by 2 Li atoms (Figure 5a). The doping is done at the interface region of NiO (<sup>Ni</sup>L<sub>1</sub>, Figure 5b) in direct contact with MAPbI<sub>3</sub> and in the bulk-like region of NiO (<sup>Ni</sup>L<sub>3</sub>, Figure 1c). Li doping at the interface-like region is 1.5 eV (0.75 eV per Li atom) more favorable than in the bulk-like region. Hence, our results indicate that the doped Li atoms would probably be distributed in NiO at the interface region being in contact with MAPbI<sub>3</sub>. Nevertheless, the other configurations cannot be completely excluded given the relatively low energy difference for the system size modeled.

The band structures of ‘Li at the interface’ (Figure 5d) and ‘Li in the bulk’ (Figure 5e) region show that Li doping facilitates a  $p$ -type conduction, while no localized band is created in the gap. The reorganization of the valence bands under the influence of Li, as shown by the PDOS (Figures S23 and S24, SI), leads to an improved VBO value that becomes slightly positive (+0.00 eV for Li at the ‘interface’ region and +0.05 eV at the ‘bulk’ one, Figure 5f,g). Therefore, Li doping recovers an ideal valence energy alignment obtained with  $V_{\text{Ni}}$  while suppressing the presence of non-dispersive mid-gap states. Since dopants are not always evenly distributed in the materials, we also consider a model in which the 2 substituted Ni atoms are only separated by one O atom (Figures S23 and S24, SI). This configuration could be viewed as a well controlled NiO doped system with a high concentration of Li in a confined region of the material. Energetically, the original ‘spread’ model is 0.3 eV (0.15 eV per Li

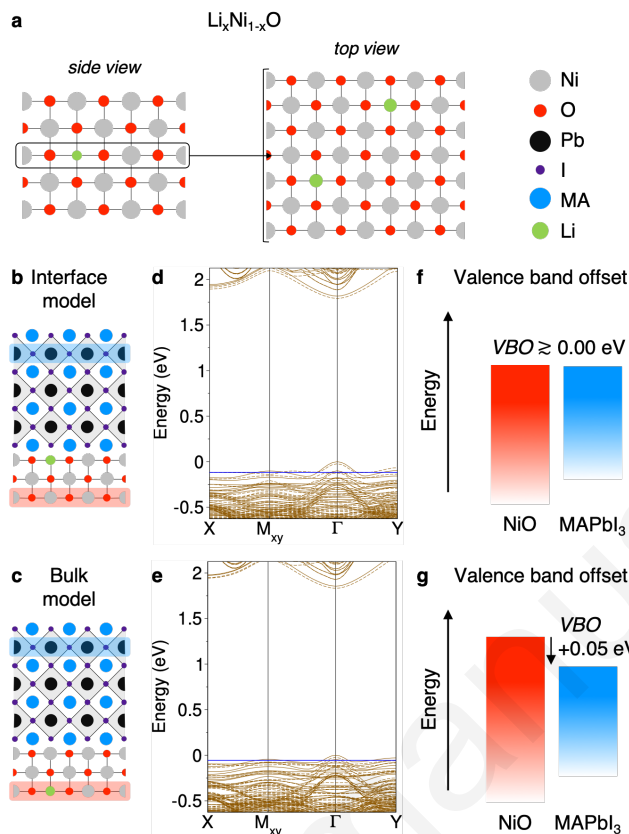


Figure 5: Role of Li doping in the NiO/MAPbI<sub>3</sub> interface. **a**  $\text{Li}_x\text{Ni}_{1-x}\text{O}$  models with dopants spread across a NiO layer. **b** ‘Interface’ model where the doped layer is at the interface. **c** ‘Bulk’ model where the dopants are placed in the bulk-like layer. Calculated band structures of the **d** ‘interface’ and **e** ‘bulk’ models. The valence band maximum at the  $\Gamma$  point is taken as the energy reference, a blue line marks the Fermi level. Plain and dashed lines correspond to majority and minority spins, respectively. **f, g** Corresponding computed valence band offsets. Both situations lead to a favorable hole extraction.

atom) more favorable than the clustered one at both the interface-like and bulk-like regions. We notice that VBO shift increases when Li atoms are clustered in a confined space resulting in +0.31 eV and +0.26 eV values at the interface-like and bulk-like regions, respectively. We also examined the effect of increased dopant concentration by substituting 4 Ni atoms by Li atoms, bringing the concentration to 5%. Again, we examined configurations where Li atoms are ‘clustered’ in one layer and spread across two NiO layers (Figure S25, SI). Here, VBO varies from +0.21 eV when Li atoms are “clustered” to +0.15 eV when they are ‘spread’ (Figure S25, SI). This suggests that 5% Li content in NiO should improve the conversion efficiency of the HOP device as a result of increased open circuit voltage.



1  
2  
3 The calculated improved energy level alignment of NiO doped Li with MAPbI<sub>3</sub> is in  
4 agreement with the enhanced efficiency of LiNiO<sub>x</sub>/MAPbI<sub>3</sub> devices as compared to undoped  
5 NiO.<sup>18,71</sup> The PDOS of the different systems with Li doping shows that the introduction of  
6 Li pushes NiO states to the same energy level or above those of MAPbI<sub>3</sub> while reinforcing  
7 their hybridization at the valence band maximum (Figures S26, SI). At the same time, Li  
8 states remain about 0.5 eV below (Figure S26, SI). The net effect results in a doped NiO  
9 being a better hole transport layer.  
10  
11

12  
13 Interestingly, we obtained an increased VBO ( $\geq 0.00$  eV) of NiO/MAPbI<sub>3</sub> heterostructure  
14 when NiO is doped with Rb and Cs atoms (Figures S27 and S28, SI). As with Li, their  
15 insertion into NiO enhances the hybridization between MAPbI<sub>3</sub> and the HTL. With Rb  
16 doping, we calculated a VBO of +0.46 eV (Figure S27, SI). For Cs, we calculated a VBO  
17 of +0.41 eV (Figure S28, SI). The large atomic size of Rb and Cs induces more structural  
18 relaxation at the interface causing an increase of VBO. Given that Cs and Rb are already  
19 adopted as cations in mixed-cation 3D HOP,<sup>16,33</sup> they may be considered as alternative  
20 dopants of NiO in the search of optimizing the efficiency of MAPbI<sub>3</sub> solar devices.  
21  
22  
23  
24  
25  
26  
27  
28  
29  
30  
31  
32  
33  
34

## 35 Conclusions

36  
37 In summary, we demonstrate the role of native defects and doping on the energetics and  
38 charge carrier extraction for devices based on NiO interfaces. Our computed valence band  
39 offsets are consistent with experimental UPS absolute valence band energies of NiO. More-  
40 over, our analysis clarifies the experimentally reported ideal valence band alignment between  
41 MAPbI<sub>3</sub> and NiO, which is related to the intrinsic Ni vacancies of the hole transporting ma-  
42 terial. The appearance of these dominant Ni-vacancies is commensurate with experimental  
43 report on standard NiO processing conditions.<sup>62</sup> Furthermore, we highlight the effect of Li  
44 doping in NiO to reach improved energy alignment of the perovskite-NiO interface foster-  
45 ing enhanced hole extraction. Hence, we propose alternatives to Li doping of NiO such  
46 as Cs or Rb to further fine-tune the NiO interfacial energetics. Additionally, we highlight  
47  
48  
49  
50  
51  
52  
53  
54  
55  
56  
57  
58  
59  
60

1  
2  
3 the importance of the dielectric mismatch. For instance, the dielectric properties related to  
4 the high-frequency component of the interface indicate a low dielectric mismatch between  
5 MAPbI<sub>3</sub> and NiO, which benefits hole collection. The combined results bring together a  
6 holistic picture on the interfacial properties of NiO. Our findings open avenues for the opti-  
7 mization of thin-film devices based on NiO contacts, and help the reader to adopt relevant  
8 theoretical strategies to model the properties of heterostructures.  
9  
10  
11  
12  
13  
14  
15  
16

## 17 **Supporting Information Available**

18  
19  
20 Computational details; Electronic structure of NiO; Detailed description of the construction  
21 of the interface models; Energy level alignment using Hartree potential profiles; Additional  
22 plane-wave calculations on valence band energy level alignments; Effects of MAPbI<sub>3</sub> surface  
23 termination and substituting MA cation on the valence band offset of MAPbI<sub>3</sub>/NiO; Pro-  
24 jected density of states for systems with vacancies or dopants; Band structures for systems  
25 with dopants;  
26  
27  
28  
29  
30  
31  
32  
33  
34

## 35 **Acknowledgement**

36  
37  
38 ISCR and FOTON have received funding from the European Union's Horizon 2020 program,  
39 through a FET Open research and innovation action under the grant agreement No 687008.  
40 The work at the Institut des Sciences Chimiques de Rennes was supported by Agence Na-  
41 tionale pour la Recherche (TRANSHYPERO project). J.E. acknowledges financial support  
42 from the Institute Universitaire de France. This work was performed, in part, at the Center  
43 for Integrated Nanotechnologies, a U.S. Department of Energy, Office of Science User Facil-  
44 ity. S.T. acknowledges support of LANL LDRD program. This work was granted access to  
45 the HPC resources of [TGCC/CINES/IDRIS] under the allocations 2016-x2016097682/2017-  
46 A0010907682/2018-A0010907682 made by GENCI.  
47  
48  
49  
50  
51  
52  
53  
54  
55  
56  
57  
58  
59  
60

## References

- (1) Sherkar, T. S.; Koster, L. J. A. Dielectric Effects at Organic/Inorganic Interfaces in Nanostructured Devices. *ACS Appl. Mater. Interfaces* **2015**, *7*, 11881–11889.
- (2) Schulz, P.; Cahen, D.; Kahn, A. Halide Perovskites: Is It All about the Interfaces? *Chem. Rev.* **2019**, *119*, 3349–3417.
- (3) Chueh, C.-C.; Li, C.-Z.; Jen, A. K.-Y. Recent Progress and Perspective in Solution-Processed Interfacial Materials for Efficient and Stable Polymer and Organometal Perovskite Solar Cells. *Energy Environ. Sci.* **2015**, *8*, 1160–1189.
- (4) Yip, H.-L.; Jen, A. K.-Y. Recent Advances in Solution-Processed Interfacial Materials For Efficient And Stable Polymer Solar Cells. *Energy Environ. Sci.* **2012**, *5*, 5994–6011.
- (5) Steirer, K. X.; Chesin, J. P.; Widjonarko, N. E.; Berry, J. J.; Miedaner, A.; Ginley, D. S.; Olson, D. C. Solution Deposited NiO Thin-Films As Hole Transport Layers in Organic Photovoltaics. *Org. Elec.* **2010**, *11*, 1414–1418.
- (6) He, J.; Lindström, H.; Hagfeldt, A.; Lindquist, S.-E. Dye-Sensitized Nanostructured Tandem Cell-First Demonstrated Cell With a Dye-Sensitized Photocathode. *Sol. Energy Mater Sol. Cells* **2000**, *62*, 265–273.
- (7) Irwin, M. D.; Buchholz, D. B.; Hains, A. W.; Chang, R. P. H.; Marks, T. J. p-Type Semiconducting Nickel Oxide As An Efficiency-Enhancing Anode Interfacial Layer In Polymer Bulk-Heterojunction Solar Cells. *Proc. Natl. Acad. Sci. U.S.A.* **2008**, *105*, 2783–2787.
- (8) Sato, H.; Minami, T.; Takata, S.; Yamada, T. Transparent Conducting p-Type NiO Thin Films Prepared By Magnetron Sputtering. *Thin Solid Films* **1993**, *236*, 27–31.
- (9) Kato, H.; Asakura, K.; Kudo, A. Highly Efficient Water Splitting into H<sub>2</sub> and O<sub>2</sub> over Lanthanum-Doped NaTaO<sub>3</sub> Photocatalysts with High Crystallinity and Surface Nanostructure. *J. Am. Chem. Soc.* **2003**, *125*, 3082–3089.
- (10) Varghese, B.; Reddy, M. V.; Yanwu, Z.; Lit, C. S.; Hoong, T. C.; Subba Rao, G. V.; Chowdari, B. V. R.; Wee, A. T. S.; Lim, C. T.; Sow, C.-H. Fabrication of NiO Nanowall Electrodes for High Performance Lithium Ion Battery. *Chem. Mater.* **2008**, *20*, 3360–3367.
- (11) <https://www.nrel.gov/pv/cell-efficiency.html>, Accessed: 15-10-2019.
- (12) You, J.; Meng, L.; Song, T.-B.; Guo, T.-F.; Yang, Y. M.; Chang, W.-H.; Hong, Z.; Chen, H.; Zhou, H.; Chen, Q.; Liu, Y.; De Marco, N.; Yang, Y. Improved Air Stability of Perovskite Solar Cells Via Solution-Processed Metal Oxide Transport Layers. *Nature Nanotech.* **2016**, *11*, 75–81.
- (13) Chen, W.; Wu, Y.; Yue, Y.; Liu, J.; Zhang, W.; Yang, X.; Chen, H.; Bi, E.; Ashraful, I.; Grätzel, M.; Han, L. Efficient and Stable Large-Area Perovskite Solar Cells with Inorganic Charge Extraction Layers. *Science* **2015**, *350*, 944–948.
- (14) Seo, S.; Park, I. J.; Kim, M.; Lee, S.; Bae, C.; Jung, H. S.; Park, N.-G.; Kim, J. Y.; Shin, H. An Ultra-Thin, Un-Doped NiO Hole Transporting Layer of Highly Efficient (16.4%) Organic-Inorganic Hybrid Perovskite Solar Cells. *Nanoscale* **2016**, *8*, 11403–11412.

- 1  
2  
3  
4 (15) Bush, K. A. et al. 23.6%-Efficient Monolithic Perovskite/Silicon Tandem Solar Cells with  
5 Improved Stability. *Nature Energy* **2017**, *2*, 17009.
- 6  
7 (16) Tsai, H.; Asadpour, R.; Blancon, J.-C.; Stoumpos, C. C.; Durand, O.; Strzalka, J. W.; Chen, B.;  
8 Verduzco, R.; Ajayan, P. M.; Tretiak, S.; Even, J.; Alam, M. A.; Kanatzidis, M. G.; Nie, W.;  
9 Mohite, A. D. Light-Induced Lattice Expansion leads to High-Efficiency Perovskite Solar Cells.  
10 *Science* **2018**, *360*, 67–70.
- 11  
12 (17) Chen, W.; Wu, Y.; Liu, J.; Qin, C.; Yang, X.; Islam, A.; Cheng, Y.-B.; Han, L. Hybrid  
13 Interfacial Layer Leads To Solid Performance Improvement of Inverted Perovskite Solar Cells.  
14 *Energy Environ. Sci.* **2015**, *8*, 629–640.
- 15  
16 (18) Nie, W.; Tsai, H.; Blancon, J.-C.; Liu, F.; Stoumpos, C. C.; Traore, B.; Kepenekian, M.;  
17 Durand, O.; Katan, C.; Tretiak, S.; Crochet, J.; Ajayan, P. M.; Kanatzidis, M.; Even, J.; Mo-  
18 hite, A. D. Critical Role of Interface and Crystallinity on the Performance and Photostability  
19 of Perovskite Solar Cell on Nickel Oxide. *Adv. Mater.* **2018**, *30*, 1703879.
- 20  
21 (19) Mosconi, E.; Ronca, E.; De Angelis, F. First-Principles Investigation of the TiO<sub>2</sub>/Organohalide  
22 Perovskites Interface: The Role of Interfacial Chlorine. *J. Phys. Chem. Lett.* **2014**, *5*, 2619–  
23 2625.
- 24  
25 (20) Li, L.; Mi, J.; Yong, Y.; Mao, B.; Shi, W. First-Principles Study On the Lattice Plane And  
26 Termination Dependence of the Electronic Properties of the NiO/CH<sub>3</sub>NH<sub>3</sub>PbI<sub>3</sub> Interfaces. *J.*  
27 *Mater. Chem. C* **2018**, *6*, 8226–8233.
- 28  
29 (21) Du Plessis, P. de V.; van Tonder, S. J.; Alberts, L. Elastic Constants of a NiO Single Crystal:  
30 I. *J. Phys. C: Solid State Phys.* **1971**, *4*, 1983–1987.
- 31  
32 (22) Li, J.-L.; Rignanese, G.-M.; Louie, S. G. Quasiparticle Energy Bands of NiO in the GW  
33 Approximation. *Phys. Rev. B* **2005**, *71*, 193102.
- 34  
35 (23) Jiang, H.; Gomez-Abal, R. I.; Rinke, P.; Scheffler, M. First-Principles Modeling of Localized  
36 *d* States with the GW/LDA+U Approach. *Phys. Rev. B* **2010**, *82*, 045108.
- 37  
38 (24) Panda, S. K. et al. High Photon Energy Spectroscopy of NiO: Experiment and Theory. *Phys.*  
39 *Rev. B* **2016**, *93*, 235138.
- 40  
41 (25) Rohrbach, A.; Hafner, J.; Kresse, G. Molecular Adsorption on the Surface of Strongly Cor-  
42 related Transition-Metal Oxides: A Case Study For CO/NiO(100). *Phys. Rev. B* **2004**, *69*,  
43 075413.
- 44  
45 (26) Anisimov, V. I.; Aryasetiawan, F.; Lichtenstein, A. I. First-Principles Calculations of the  
46 Electronic Structure And Spectra of Strongly Correlated Systems: the LDA+U Method. *J.*  
47 *Phys.: Condens. Matter* **1997**, *9*, 767–808.
- 48  
49 (27) Dudarev, S. L.; Botton, G. A.; Savrasov, S. Y.; Humphreys, C. J.; Sutton, A. P. Electron-  
50 Energy-Loss Spectra And the Structural Stability of Nickel Oxide: An LSDA+U Study. *Phys.*  
51 *Rev. B* **1998**, *57*, 1505–1509.
- 52  
53 (28) Soler, M.; Artacho, E.; Gale, J. D.; Garc, A.; Junquera, J.; Ordejon, P.; Daniel, S. The SIESTA  
54 Method for Ab Initio Order-N Materials. *J. Phys.: Condens. Matter* **2002**, *14*, 2745–2779.
- 55  
56  
57  
58  
59  
60

- 1  
2  
3  
4 (29) Artacho, E.; Anglada, E.; Diéguez, O.; Gale, J. D.; García, A.; Junquera, J.; Martin, R. M.;  
5 Ordejón, P.; Pruneda, J. M.; Sánchez-Portal, D.; Soler, J. M. The SIESTA Method; Develop-  
6 ments and Applicability. *J. Phys.: Condens. Matter* **2008**, *20*, 064208.
- 7  
8 (30) Cococcioni, M.; de Gironcoli, S. Linear Response Approach to the Calculation of the Effective  
9 Interaction Parameters in the LDA + U Method. *Phys. Rev. B* **2005**, *71*, 035105.
- 10  
11 (31) Ködderitzsch, D.; Hergert, W.; Temmerman, W. M.; Szotek, Z.; Ernst, A.; Winter, H. Ex-  
12 change Interactions in NiO and at the NiO(100) Surface. *Phys. Rev. B* **2002**, *66*, 064434.
- 13  
14 (32) Welton-Cook, M. R.; Prutton, M. LEED Calculations for the NiO (100) Surface: Extension  
15 to Lower Energies. *J. Phys. C: Solid State Phys.* **1980**, *13*, 3993–3400.
- 16  
17 (33) Saliba, M.; Matsui, T.; Domanski, K.; Seo, J.-Y.; Ummadisingu, A.; Zakeeruddin, S. M.;  
18 Correa-Baena, J.-P.; Tress, W. R.; Abate, A.; Hagfeldt, A.; Grätzel, M. Incorporation of  
19 Rubidium Cations Into Perovskite Solar Cells Improves Photovoltaic Performance. *Science*  
20 **2016**, *354*, 206–209.
- 21  
22 (34) Yang, W. S.; Park, B.-W.; Jung, E. H.; Jeon, N. J.; Kim, Y. C.; Lee, D. U.; Shin, S. S.; Seo, J.;  
23 Kim, E. K.; Noh, J. H.; Seok, S. I. Iodide Management in Formamidinium-Lead-Halide-Based  
24 Perovskite Layers for Efficient Solar Cells. *Science* **2017**, *356*, 1376–1379.
- 25  
26 (35) Even, J.; Carignano, M.; Katan, C. Molecular Disorder and Translation/Rotation Coupling in  
27 the Plastic Crystal Phase of Hybrid Perovskites. *Nanoscale* **2016**, *8*, 6222–6236.
- 28  
29 (36) She, L.; Liu, M.; Zhong, D. Atomic Structures of CH<sub>3</sub>NH<sub>3</sub>PbI<sub>3</sub> (001) Surfaces. *ACS Nano*  
30 **2016**, *10*, 1126–1131.
- 31  
32 (37) Quarti, C.; Mosconi, E.; De Angelis, F. Interplay of Orientational Order and Electronic Struc-  
33 ture in Methylammonium Lead Iodide: Implications for Solar Cell Operation. *Chem. Mater.*  
34 **2014**, *26*, 6557–6569.
- 35  
36 (38) Wyckoff, R. W. G. *Cadmium Chloride Structure*, 2nd ed.; Interscience Publishers, New York,  
37 New York, 1963; Vol. 1; pp 239–444.
- 38  
39 (39) Even, J.; Pedesseau, L.; Kepenekian, M. Electronic Surface States and Dielectric Self-Energy  
40 Profiles in Colloidal Nanoscale Platelets of CdSe. *Phys. Chem. Chem. Phys.* **2014**, *16*, 25182–  
41 25190.
- 42  
43 (40) Saponi, D.; Kepenekian, M.; Pedesseau, L.; Katan, C.; Even, J. Quantum Confinement and  
44 Dielectric Profiles of Colloidal Nanoplatelets of Halide Inorganic and Hybrid Organic-Inorganic  
45 Perovskites. *Nanoscale* **2016**, *8*, 6369–6378.
- 46  
47 (41) Gielisse, P. J.; Plendl, J. N.; Mansur, L. C.; Marshall, R.; Mitra, S. S.; Mykolajewycz, R.;  
48 Smakula, A. Infrared Properties of NiO and CoO and Their Mixed Crystals. *J. Appl. Phys.*  
49 **1965**, *36*, 2446–2450.
- 50  
51 (42) Hirasawa, M.; Ishihara, T.; Goto, T.; Uchida, K.; Miura, N. Magnetoabsorption of the Lowest  
52 Exciton in Perovskite-Type Compound (CH<sub>3</sub>NH<sub>3</sub>)PbI<sub>3</sub>. *Physica B Condens. Matter.* **1994**,  
53 *201*, 427–430.
- 54  
55  
56  
57  
58  
59  
60

- 1  
2  
3  
4 (43) Even, J.; Pedesseau, L.; Katan, C. Analysis of Multivalley and Multibandgap Absorption and  
5 Enhancement of Free Carriers Related to Exciton Screening in Hybrid Perovskites. *J. Phys.*  
6 *Chem. C* **2014**, *118*, 11566–11572.
- 7  
8 (44) Yang, Z.; Surrente, A.; Galkowski, K.; Bruyant, N.; Maude, D. K.; Haghighirad, A. A.;  
9 Snaith, H. J.; Plochocka, P.; Nicholas, R. J. Unraveling the Exciton Binding Energy and the  
10 Dielectric Constant in Single-Crystal Methylammonium Lead Triiodide Perovskite. *J. Phys.*  
11 *Chem. Lett.* **2017**, *8*, 1851–1855.
- 12  
13 (45) Junquera, J.; Zimmer, M.; Ordejón, P.; Ghosez, P. First-principles Calculation of The Band  
14 Offset at BaO/BaTiO<sub>3</sub> and SrO/SrTiO<sub>3</sub> Interfaces. *Phys. Rev. B* **2003**, *67*, 155327.
- 15  
16 (46) Traore, B.; Pedesseau, L.; Assam, L.; Che, X.; Blancon, J.-C.; Tsai, H.; Nie, W.;  
17 Stoumpos, C. C.; Kanatzidis, M. G.; Tretiak, S.; Mohite, A. D.; Even, J.; Kepenekian, M.;  
18 Katan, C. Composite Nature of Layered Hybrid Perovskites: Assessment on Quantum and  
19 Dielectric Confinements and Band Alignment. *ACS Nano* **2018**, *12*, 3321–3332.
- 20  
21 (47) Peressi, M.; Binggeli, N.; Baldereschi, A. Band Engineering at Interfaces: Theory And Nu-  
22 merical Experiments. *J. Phys. D: Appl. Phys.* **1998**, *31*, 1273–1299.
- 23  
24 (48) Liu, T.; Chen, K.; Hu, Q.; Zhu, R.; Gong, Q. Inverted Perovskite Solar Cells: Progresses and  
25 Perspectives. *Adv. Energy Mater.* **2016**, *6*, 1600457.
- 26  
27 (49) Niu, G.; Wang, S.; Li, J.; Li, W.; Wang, L. Oxygen Doping in Nickel Oxide For Highly Efficient  
28 Planar Perovskite Solar Cells. *J. Mater. Chem. A* **2018**, *6*, 4721–4728.
- 29  
30 (50) Heyd, J.; Scuseria, G. E.; Ernzerhof, M. Hybrid Functionals Based on a Screened Coulomb  
31 Potential. *J. Chem. Phys.* **2003**, *118*, 8207–8215.
- 32  
33 (51) Heyd, J.; Scuseria, G. E.; Ernzerhof, M. Erratum: “Hybrid Functionals Based on a Screened  
34 Coulomb Potential” [*J. Chem. Phys.* 118, 8207 (2003)]. *J. Chem. Phys.* **2006**, *124*, 219906.
- 35  
36 (52) Haruyama, J.; Sodeyama, K.; Han, L.; Tateyama, Y. Termination Dependence of Tetragonal  
37 CH<sub>3</sub>NH<sub>3</sub>PbI<sub>3</sub> Surfaces for Perovskite Solar Cells. *J. Phys. Chem. Lett.* **2014**, *5*, 2903–2909.
- 38  
39 (53) Volonakis, G.; Giustino, F. Interfaces Between Graphene-Related Materials and MAPbI<sub>3</sub>: In-  
40 sights from First-Principles. *Adv. Mater. Interfaces* **2018**, *5*, 1800496.
- 41  
42 (54) Steirer, K. X.; Schulz, P.; Teeter, G.; Stevanovic, V.; Yang, M.; Zhu, K.; Berry, J. J. Defect  
43 Tolerance in Methylammonium Lead Triiodide Perovskite. *ACS Energy Lett.* **2016**, *1*, 360–366.
- 44  
45 (55) Meggiolaro, D.; De Angelis, F. First-Principles Modeling of Defects in Lead Halide Perovskites:  
46 Best Practices and Open Issues. *ACS Energy Lett.* **2018**, *3*, 2206–2222.
- 47  
48 (56) Yavari, M. et al. How Far Does the Defect Tolerance of Lead-Halide Perovskites Range? The  
49 Example of Bi Impurities Introducing Efficient Recombination Centers. *J. Mater. Chem. A*  
50 **2019**, *7*, 23838–23853.
- 51  
52 (57) Meggiolaro, D.; Motti, S. G.; Mosconi, E.; Barker, A. J.; Ball, J.; Andrea Riccardo Perini, C.;  
53 Deschler, F.; Petrozza, A.; De Angelis, F. Iodine Chemistry Determines the Defect Tolerance  
54 of Lead-Halide Perovskites. *Energy Environ. Sci.* **2018**, *11*, 702–713.
- 55  
56  
57  
58  
59  
60

- 1  
2  
3  
4 (58) Kim, J.; Lee, S.-H.; Lee, J. H.; Hong, K.-H. The Role of Intrinsic Defects in Methylammonium  
5 Lead Iodide Perovskite. *J. Phys. Chem. Lett.* **2014**, *5*, 1312–1317.
- 6  
7 (59) Kye, Y.-H.; Yu, C.-J.; Jong, U.-G.; Chen, Y.; Walsh, A. Critical Role of Water in Defect  
8 Aggregation and Chemical Degradation of Perovskite Solar Cells. *J. Phys. Chem. Lett.* **2018**,  
9 *9*, 2196–2201.
- 10  
11 (60) Zhang, W. B.; Yu, N.; Yu, W. Y.; Tang, B. Y. Stability and Magnetism of Vacancy in NiO: A  
12 GGA+U Study. *Eur. Phys. J. B* **2008**, *64*, 153–158.
- 13  
14 (61) Osorio-Guillén, J.; Lany, S.; Zunger, A. Nonstoichiometry and Hole Doping in NiO. *AIP Conf.*  
15 *Proc.* **2010**, *1199*, 128–129.
- 16  
17 (62) Jang, W.-L.; Lu, Y.-M.; Hwang, W.-S.; Hsiung, T.-L.; Wang, H. P. Point Defects in Sputtered  
18 NiO Films. *Appl. Phys. Lett.* **2009**, *94*, 062103.
- 19  
20 (63) Kojima, A.; Teshima, K.; Shirai, Y.; Miyasaka, T. Organometal Halide Perovskites as Visible-  
21 Light Sensitizers for Photovoltaic Cells. *J. Am. Chem. Soc.* **2009**, *131*, 6050–6051.
- 22  
23 (64) Greiner, M. T.; Helander, M. G.; Wang, Z.-B.; Tang, W.-M.; Lu, Z.-H. Effects of Processing  
24 Conditions on the Work Function and Energy-Level Alignment of NiO Thin Films. *J. Phys.*  
25 *Chem. C* **2010**, *114*, 19777–19781.
- 26  
27 (65) Madjid, A. H.; Martinez, J. M. Thermionic Emission from Nickel Oxide. *Phys. Rev. Lett.* **1972**,  
28 *28*, 1313–1315.
- 29  
30 (66) Olivier, J.; Servet, B.; Vergnolle, M.; Mosca, M.; Garry, G. Stability/Instability of Conduc-  
31 tivity and Work Function Changes of ITO Thin Films, UV-Irradiated in Air or Vacuum:  
32 Measurements by the Four-Probe Method and by Kelvin Force Microscopy. *Synth. Met.* **2001**,  
33 *122*, 87–89.
- 34  
35 (67) Hu, L.; Peng, J.; Wang, W.; Xia, Z.; Yuan, J.; Lu, J.; Huang, X.; Ma, W.; Song, H.; Chen, W.;  
36 Cheng, Y.-B.; Tang, J. Sequential Deposition of CH<sub>3</sub>NH<sub>3</sub>PbI<sub>3</sub> on Planar NiO Film for Efficient  
37 Planar Perovskite Solar Cells. *ACS Photonics* **2014**, *1*, 547–553.
- 38  
39 (68) Zhai, Z.; Huang, X.; Xu, M.; Yuan, J.; Peng, J.; Ma, W. Greatly Reduced Processing Temper-  
40 ature for a Solution-Processed NiO<sub>x</sub> Buffer Layer in Polymer Solar Cells. *Adv. Energy Mater.*  
41 **2013**, *3*, 1614–1622.
- 42  
43 (69) Kamiya, T.; Ohta, H.; Kamiya, M.; Nomura, K.; Ueda, K.; Hirano, M.; Hosono, H. Li-Doped  
44 NiO Epitaxial Thin Film with Atomically Flat Surface. *J. Mater. Res.* **2004**, *19*, 913–920.
- 45  
46 (70) Jang, W.-L.; Lu, Y.-M.; Hwang, W.-S.; Chen, W.-C. Electrical Properties of Li-Doped NiO  
47 Films. *J. Eur. Ceram. Soc.* **2010**, *30*, 503–508.
- 48  
49 (71) Park, M.-A.; Park, I. J.; Park, S.; Kim, J.; Jo, W.; Son, H. J.; Kim, J. Y. Enhanced Electrical  
50 Properties of Li-Doped NiO<sub>x</sub> Hole Extraction Layer in p-i-n Type Perovskite Solar Cells. *Curr.*  
51 *Appl. Phys.* **2018**, *18*, S55–S59.
- 52  
53  
54  
55  
56  
57  
58  
59  
60

## Graphical TOC Entry

